JOURNAL OF MATERIALS SCIENCE 37 (2002) 2109–2116

Evaluation of thermocapillary driving forces in the development of striations during the spin coating process

D. E. HAAS, D. P. BIRNIE, III*
Department of Materials Science and Engineering, University of Arizona, Tucson, AZ 85721-0012, USA
E-mail: birnie@AML.arizona.edu

The evolution of a temperature gradient at the free surface of a coating solution during the spin coating process is examined. Solvent evaporation causes localized cooling at the top that can result in thermocapillary instability within the coating solution, and thereby driving convective flows that may result in non-uniform coatings. We examine the evolution of these temperature gradients by using a one dimensional finite difference model that simultaneously describes the thinning behavior (both by flow and by evaporation) and the temperature evolution within the solution. The entire system is initially isothermal but is subject to evaporation-driven cooling at the free surface of the gradually thinning fluid. The model is then used to determine the magnitude of the thermocapillary effects during the spin coating process. As test systems we simulate the spin coating of several pure alcohol solutions having different volatilities and therefore different evaporative-cooling powers. As the fluid thins, we calculate the instantaneous Marangoni (*Mn*) number, which signifies the magnitude of thermocapillary-driven convection. We compare these *Mn* values against their relevant threshold values, determined from prior reports in the literature, in order to deduce the magnitude of the instabilities they represent. If the *Mn* value is super-critical, then the instability that it represents will be sufficient for the onset of convection cells within a stagnant fluid layer of corresponding thickness. Because the radial outflow is fully laminar under normal conditions, super-critical *Mn* values imply that similar instabilities would arise within a spinning solution. Super-critical *Mn* values were observed under numerous conditions suggesting that thermocapillary instability may be responsible for striation features that develop in coatings made by spin coating. Trends related to spin-speed, solvent volatility, and initial solution thickness are discussed with the goal of improving the flatness of coatings that are made by this process.

Nomenclature

ρ	Density (g/cm^3)
ω	Spin speed (rpm)
η	Viscosity (Pa · s)
k	Thermal conductivity (W/(°C · m))
C	Specific heat capacity (J/(kg · °C))
α	$k/(\rho \cdot C)$ Thermal diffusivity (m^2/s)
β	Thermal volumetric expansivity (1/°C)
v	Kinematic viscosity (m^2/s)
g	Acceleration due to gravity (m/s^2)
$\frac{\partial \sigma}{\partial T}$	Change in surface tension w/temperature (J/(m^2 · °C))
L	Latent heat of evaporation (J/g)
e	Evaporation rate (μ/s)
C_e	Evaporation rate proportionality constant (μ/s)(rpm$^{-1/2}$) [$e = C_e\sqrt{\omega}$] [17]
H	Thickness of film layer (cm)

1. Introduction

The spin coating process is a simple method for depositing thin layers of material onto nominally flat surfaces. The substrate is flooded with coating solution (containing coating constituents as well as solvents). The solution spreads outward due to centrifugal effects, eventually leaving a thin layer covering the entire substrate surface. The thickness, homogeneity and uniformity of this final film are governed by many factors, including the volatility of the constituents in the precursor solution. In this paper we examine how the solvent's volatility may contribute to coating non-uniformities as a result of temperature differences caused by evaporative cooling. Evaporative cooling is already known to be responsible for "chuck-mark" defects [1, 2], so examining the connection between the evaporative cooling and other coating defects is warranted and might

*Author to whom all correspondence should be addressed.

help develop improved techniques for depositing higher quality coatings in the future.

In many cases spin-on coatings are substantially uniform across the entire substrate, however certain surface defects do sometimes occur. "Striations" are one of the most common surface defects that can occur in spin-on thin films. They appear as radially oriented thickness undulations that emanate spoke-like from the center of the substrate. Whereas, the center of the substrate displays a cellular thickness pattern reminiscent of Bénard cells. Striation development during the coating of photoresists for IC manufacturing has been shown to result in electrical bit failures due to the dimensional variations induced by these surface ripples [3]. The actual mechanism by which striations develop during the spin coating process is not presently known, although one recent study [4] has demonstrated a direct link between the evaporation of volatile solvents during the thinning process and the development of this particular type of surface defect. Their work showed that spinning in a solvent-saturated environment (thus preventing evaporation) created substantially flatter coatings. However, the physical process driven by the solvent evaporation was not determined in their work.

Two primary effects can easily be caused by the solvent evaporation. First, the solvent evaporation can cause a composition gradient near the surface of the still-flowing solution during the spin coating process (because the coating constituents are left behind when the solvent evaporates). The second effects is the active evaporative cooling (mentioned above), again acting at the free surface of the solution during its radial outflow. Either of these effects could (and both probably do) cause problems in the coating formation process.

The ability of these two physical processes to create surface ripples in coatings is related to the processes involved in classical Bénard cell formation (as discussed in further detail below). Although buoyant forces can play a role, the primary influence that these phenomena have is through their effect on surface tension [5, 6]. Surface tension is usually lower in mixtures or at higher temperatures, so the removal of solvents can cause a localized increase in surface tension through either compositional or temperature grounds. The generation of such gradients in surface tension across the surface causes the fluid to become physically unstable. As a starting point in understanding these effects, we focus our attention on the thermocapillary instabilities that may develop. In future work we hope to extend our findings to include possible soluto-capillary effects and instabilities.

2. Background

In order to address evaporative cooling effects upon rotating solutions it is useful to first examine instability processes that occur in stationary fluid layers. At the turn of the century Bénard [7] noticed the development of a uniform convection pattern within thin layers of fluid that were open to the ambient and heated from below. This phenomenon, now known as Bénard convection, has been well documented and studied throughout the last century. The convection pattern that results can appear as uniformly spaced hexagonal dimples across the thin film surface [8]. These convection cells were initially attributed to buoyancy effects [9] that result from warmer fluid near the bottom rising up and displacing the cooler fluid near the surface, ultimately creating a circulation effect in the liquid. Subsequent studies have shown that in many cases (including those actually studied by Bénard himself) these convection cells are not strictly buoyancy-driven but rather are the result of surface tension variations across the fluid surface [5, 6] causing a similar fluid circulation process. Thus, buoyancy effects cannot account for the development of convection cells within fluids that are on the order of 1 mm or less [5, 6]. Within this thinner regime, surface tension affects are found to be dominant.

As stated above, the evaporation of solvents from solution results in a net cooling effect at the fluid/air interface altering surface tension across the fluid surface. High-tension regions draw fluid away from lower tension regions resulting in a continuous convection pattern that appears as symmetrically spaced dimples across the fluid surface. These capillary effects are collectively referred to as the "Marangoni Effect", whether they arise from thermal or compositional sources. In the case of Marangoni instability resulting from *thermo*capillary forces, a "Marangoni number", *Mn*, has been devised by Pearson [6] in 1958. *Mn* is used to evaluate the significance of thermocapillary effects upon the development of convection cells:

$$Mn = \frac{\left(\frac{\partial \sigma}{\partial T}\right) H^2 \nabla T}{\eta \alpha} \tag{1}$$

where H and ∇T are the total solution depth and the thermal gradient which develops within, respectively, and the other parameters have their typical meanings and are explained in the nomenclature list on the previous page.

It is important to note that the classical thermocapillary convection process is predicated on the assumption that the temperature gradient is linear through the entire depth of the fluid—i.e. that the gradient is $\Delta T/H$, where ΔT is the bottom-to-top temperature difference experienced by the fluid. However, the conditions experienced during spin coating are dramatically transient in nature, especially with respect to the temperature gradients that can result. The evaporation of the solvent occurs at the top surface, thus simultaneously removing heat and mass from the system at that same interface. Then, heat must flow from the interior of the fluid upward in response to the evaporative cooling at the surface. Under most circumstances the temperatures profile through the depth of the coating solution will be highly non-uniform with a much steeper temperature gradient near the surface compared to that found deeper in the bulk. Thus, the region of film depth that experiences a concrete temperature gradient will be much smaller than the total coating depth, but the magnitude of that local temperature gradient might be substantial.

To consider this transient surface temperature gradient and its effect on the two types of convection we define a new parameter d that represents the effective thermal penetration depth into the surface. It characterizes

the depth over which the majority of the temperature drop, ΔT, is felt within the fluid layer. If d approaches the scale of the fluid layer's depth, H, then we return to the classical linear-gradient description above. Determination of d and ΔT in the transient case is done numerically, as described further below.

Currie [10] and Vidal and Acrivos [11] have applied this concept of a surface gradient to the Marangoni convection process. Implicit in their equations is that the capillary forces applied to the system will cause convection that rotates through the entire depth, H, of the coating solution even though the driving force is essentially exerting itself only through a surface layer depth, d. This is valid for thermocapillary effects since the underlying fluid is responding to lateral surface tractions and hydrostatic pressures that develop and the viscosity of the liquid is assumed to be relatively independent of temperature. For our calculation purposes *Mn* is recast in the manner described before [11].

$$Mn = \frac{\left(\frac{\partial \sigma}{\partial T}\right) H^2 \left(\frac{\Delta T}{d}\right)}{\eta \alpha}. \qquad (2)$$

The relationship between the formation of striations during the spin coating process and the development of convection instabilities has been investigated in the past by Daniels *et al*. [12]. They proposed that the physical parameters responsible for these convection cells within stagnant fluid layers facilitate the onset of striations within spun-on coatings. As an aside, it should be noted that Daniels *et al*. eliminated the possibility of buoyant effects from consideration; they performed a clever spin coating test by running with the substrate oriented *vertically*, rather than the normal horizontal orientation, thus removing any gravitational effects and nullifying any buoyancy driven contributions to convective flow. They found that striation defects *still occurred* across these vertically oriented spun-on solutions demonstrating that buoyancy effects were not the cause of striation development for their coating solutions. Thus their findings are compatible with the emphasis of the present work. As noted above, we examine the possibility that temperature gradients near the surface couple with a temperature-dependent surface tension, $\sigma(T)$, to drive thermocapillary convection during coating formation.

We perform a computer simulation that maps the realistic fluid thinning behavior during the spin-on process and simultaneously calculates the temperature gradients set up during the thinning process as a result of evaporative cooling of the solvent. We use this model to evaluate the likelihood that convection effects will develop during the spin coating process in response to the temperature-dependent surface tension effect. A finite difference approach is used where the total thickness of coating solution is split into a number of infinitesimal layers and small time steps are used to gradually follow the behavior during an entire spinning run. The details of this computer model are given in the next section. At each incremental time step the total film thickness, H, the localized temperature gradient depth, d, and the local temperature drop, ΔT, are quantified and values for *Mn* are calculated according to Equation 2 above. These values are then interpreted according to previously published results. In detail we compare our *Mn* values with threshold or critical values for these constants. These critical values are identified by "*Mc*" in our following discussion. We are unaware of any previous study predicting the effects of rotation upon the critical Marangoni number, thus, in order to interpret the *Mn* results of our model we compare them with thresholds applicable to stagnant fluid layers. A study performed by Vidal and Acrivos [11] determines the critical Marangoni number (*Mc*) for thin layers of 1-propanol at any given thermal gradient within the film layer. They establish a (theoretical) critical Marangoni curve that provides an estimation of the value for *Mc* at any thermal penetration depth d. In order to utilize their results we simulated the spin coating of a pure 1-propanol solution and compared the *Mn* values generated by our model to the expected *Mc* values derived in their study.

The Vidal and Acrivos study is potentially illuminating for the case of a 1-propanol solution and is the motivation behind simulating just such a solution, but in order to test the significance of other solutions we turn to more general results. Specifically we use the results of Nield [13]. This study by Nield provides theoretical critical *Mc* values that develop within a stagnant fluid layer with a rigid boundary below and free at the top surface, as we have in this case. These values are determined for a variety of different dimensionless heat transfer coefficients, $h_{tr}H/k$, where h_{tr} is the heat transfer coefficient between the fluid and the air above, H is the fluid thickness and k is the thermal conductivity of the fluid. For the fluids tested in the present work the *Mc* values were all around 80, while the calculated *Mn* values ranged over several orders of magnitude, straddling this threshold. Comparing our calculated *Mn* values against those of Nield provides a quantitative evaluation of the significance of the thermocapillary effects upon the development of convection cells during spin coating, as discussed further in the discussion section.

3. Numerical analysis

For the present study, we limit our analysis to a single component fluid† [14]. This eliminates solution composition effects on the surface tension. In addition, it avoids having to include the complex diffusion processes of various molecules, polymer chains, and/or particles throughout the fluid itself. We shall expand our analysis to include such soluto-capillary effects in future work. Because of the relatively thin fluid layer and the rotation rates typically used in real situations, we are safe to consider the fluid flow to be strictly laminar in nature. In addition, we apply the fact (as others have [15]) that the flow is almost strictly radial in direction, which thus eliminates any vertically or tangentially directed fluid flow from our calculations. The large ratio of wafer size to fluid layer thickness

†This limitation is valid because in earlier experimental studies of the absolute evaporation rate we have shown that the change in composition imposed by solvent removal is quite small, at least until the very end when the coating is close to "setting": see [14].

validates the first limitation, while the fact that striations point directly outward validates the second. The relatively low thermal conductivity values found for typical solvents suggests that heat flow through the fluid will be slow enough that only strictly vertical flow of heat will need to be considered. This simplifies a potentially complicated three-dimensional diffusion problem into a relatively simple one-dimensional situation. Such a simplification is further supported when the entire film thickness is taken into consideration. The fluid layer remains quite thin compared to the wafer diameter, thus the use of a one dimensional temperature coordinate should be sufficient, especially once we consider heat flow between extremely thin sublayers within the fluid.

In their seminal analysis in 1958, Emslie, Bonner, and Peck [15] derived equations that describe the flow of a Newtonian fluid across a rotating disk. They modeled the situation where the centrifugal rotation forces are exactly balanced by the viscous dissipation effects. Thus:

$$-\eta\frac{\partial^2 v}{\partial z^2} = \rho\omega^2 r \tag{3}$$

Solving this equation, they were able to deduce the following depth dependence of the radial velocity:

$$v_r = \frac{\rho\omega^2 r}{\eta}\left(-\frac{z^2}{2} + Hz\right). \tag{4}$$

We use this definition to describe the velocity of fluid a distance z above the substrate within a solution layer of overall thickness H.

The fluid is envisioned to be deposited uniformly atop a smooth substrate surface with a total initial thickness $H = H_o$. For computational purposes the fluid is divided into n sublayers each of equivalent initial thickness h_i such that $H_o = \Sigma h_i$, as shown in Fig. 2. The thinning of the entire fluid layer results from the combined thinning of these sublayers, each of which thins at a rate dependent upon its instantaneous distance above the stationary substrate. In addition to this rigorous simulation of the viscous flow behavior, we incorporate the evaporation effect by removing material at the appropriate rate from the top-most sublayer, $h_{i\,\max}$. In order to describe the thinning rate of a given sublayer h_i we consider the difference in mass flow into and out of an annulus of inner radius r, as shown in Fig. 1. The mass flow W is defined to be $W = \rho A v(r)$.

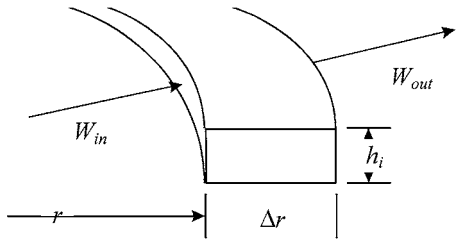

Volume of annulus = $2\pi r\Delta r h_i$

mass flow rate: $W = \rho A v(r) = \rho 2\pi r h_i v(r)$

Figure 1 Schematic representation of mass flow into and out of an annulus at radius r. Each incremental layer, h_i, has similar components that depend on height, z.

The difference in mass flow into the annulus, at radius r, and that out of the annulus, at radius $r + \Delta r$, determines the overall change in volume of the annulus. And, since the width of the annulus (Δr) must remain the same, this translates into some finite amount of thickness reduction contributed by this height increment, h_i. This results in an expression for the degree to which a given sublayer h_i, a distance z above the substrate, thins in an amount of time Δt:

$$\Delta h_i = -\frac{\rho\omega^2}{\eta}\left(Hz - \frac{1}{2}z^2\right)(1 + \Delta r/2r)h_i\Delta t. \tag{5}$$

The top sublayer undergoes thinning that is identical to other layers except for an additional term due to evaporation of solvent at the free surface, giving this expression:

$$\Delta h_{i\,\max} = -\frac{\rho\omega^2}{\eta}\left(Hz - \frac{1}{2}z^2\right)(1 + \Delta r/2r)h_{n\,\max}\Delta t - e\Delta t. \tag{6}$$

The additional $e\Delta t$ term compensates for solvent evaporation; e represents the evaporation rate (strictly an evaporation velocity in units of μ/s). As can be seen from analysis of Equations 5 and 6, sublayers farther above the substrate thin at a faster rate than those near the substrate surface, with the topmost sublayer $h_{i\,\max}$ thinning the quickest (as a result of the faster radial flow velocity at higher z values). The total thickness of the fluid layer at any time is the sum of these instantaneous sublayer thickness $H = \Sigma h_i$. Fig. 2 emphasizes this differential thinning effect, with upper layers thinning more rapidly than lower ones.

At the same time the program calculates the temperature T_i associated with the ith sublayer. As mentioned earlier, the flow of heat through the fluid is safely considered to be strictly in the vertical (z) direction. Because of the evaporative cooling perturbing the initially isothermal system, the heat flows generally upward from the substrate toward the fluid/vapor interface to compensate for evaporation at the fluid surface. Considering only a one dimensional heat flow simplifies the three-dimensional thermal diffusion equation: $\frac{\partial T}{\partial t} = \alpha\nabla^2 T$ into its one dimensional form:

$$\frac{\partial T}{\partial t} = \alpha\frac{\partial^2 T}{\partial z^2} \tag{7}$$

Equation 7 is solved numerically for each new T_i value using a finite difference approach, where care is taken to compensate for the differences in thickness between the sublayer above (h_{i+1}) and below (h_{i-1}) the ith sublayer of interest:

$$T_{i,\text{new}} = T_{i,\text{old}} + \frac{2\alpha\Delta t}{h_{i+1} + h_{i-1}}\left(\frac{T_{i+1} - T_i}{h_{i+1}} - \frac{T_i - T_{i-1}}{h_{i-1}}\right) \tag{8}$$

Since both the temperature of the atmosphere above the fluid and the evaporation of solvent itself are expected to influence the temperature evolution of the top-most layer, we employ a slightly different approach in the calculation of $T_{i\,\max}$, the temperature at the fluid/air interface. Therefore two additional terms must be included

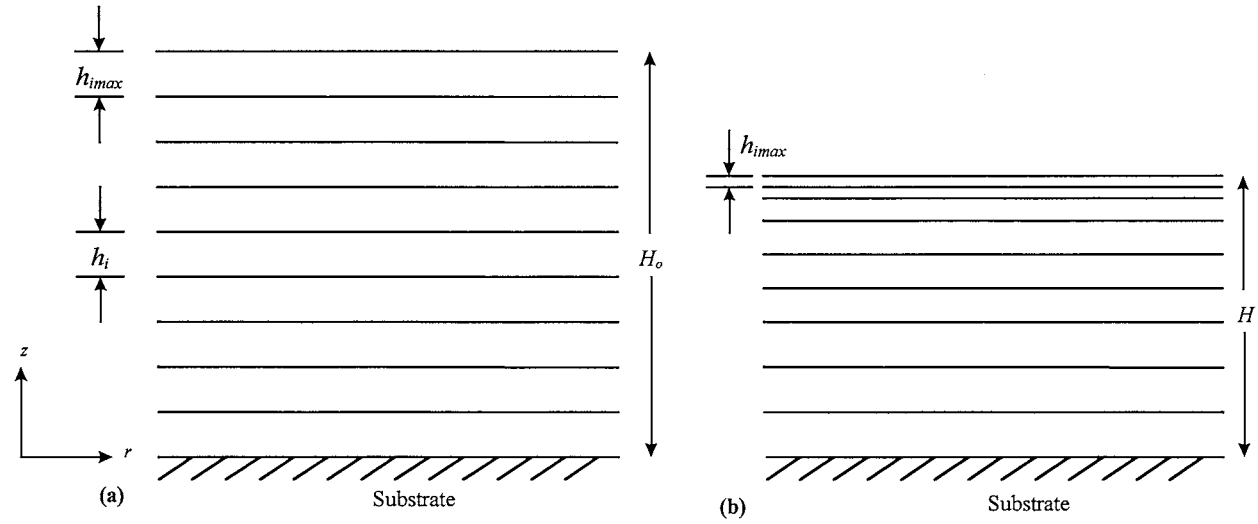

Figure 2 Schematic representation of the thinning behavior experienced by the system during spin coating. Fluid layer is broken into imax sublayers, each of initial thickness h_i as shown in (a). The sublayers thin at a rate dependent upon the height above the substrate, as given by Equation 5. Thus, sublayers farther above substrate will thin faster than those nearer the substrate, resulting in a sublayer stack like that illustrated in (b) after some finite amount of time has passed.

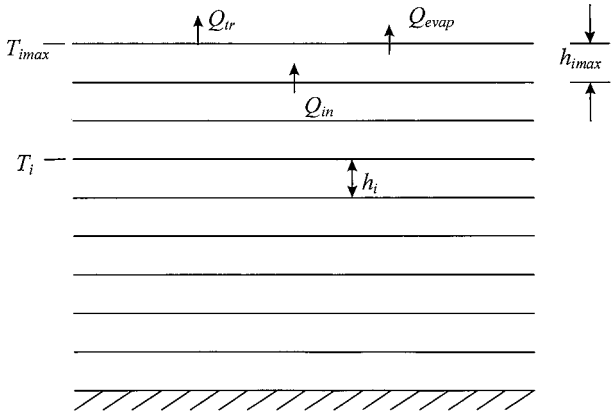

Figure 3 Simple depiction of heat flow between fluid sublayers. At the top surface of the top layer heat flows to the surroundings via evaporation of solvent material as well via heat conduction to the air flowing above the sample.

to allow accurate evaluation of the temperature evolution of the top thickness element. These terms and their directions are illustrated in Fig. 3. First we examine the heat flow coming from the layer below. This is:

$$Q_{in} = -Ak\frac{T_{i\,\max} - T_{i\,\max-1}}{h_{i\,\max}} \tag{9}$$

The heat flow from the topmost sublayer, Q_{out}, is a combination of the heat transferred from the fluid to (or from) the air by normal convection (Q_{tr}) and the heat carried away by the mass of evaporating solvent (Q_{evap}). That is $Q_{\text{out}} = Q_{\text{tr}} + Q_{\text{evap}}$. This convection term is particularly important because this effect will be present under all circumstances—with heat flowing from warmer to colder medium. In this case, with evaporative cooling of the top-most layer of the coating then assuming isothermal starting conditions, we find that the surroundings will be conducting heat back into the surface layer from both above and below. These two top-surface additional energy terms are defined below:

$$Q_{\text{tr}} = -h_{\text{tr}}A(T_\infty - T_{i\,\max}) \quad \text{and} \quad Q_{\text{evap}} = mL \tag{10}$$

where: h_{tr} heat transfer coefficient between fluid and air, T_∞ temperature of air some distance away from fluid surface; room temperature, L latent heat of evaporation for fluid, and m amount of solvent evaporated. Noted that the amount of solvent evaporated, m, is tied directly to the evaporation rate, e, used above in Equation 6.

The heat transfer coefficient is calculated according to the following equation, established by Cobb and Saunders [16] for a disk rotating in air:

$$h_{\text{tr}} = 0.336\left(\frac{k}{R}\right)\sqrt{Re}$$

where R is the radius of the substrate and Re is the Reynolds number corresponding to air flow over a rotating disk, $Re = \frac{R^2\omega}{v}$. This equation for the heat transfer coefficient has been shown to be experimentally valid for laminar airflow regimes [16] to which all simulations carried out in this present study adhere. The temperature at the fluid/air interface is therefore calculated according to:

$$T_{i\,\max,\,\text{new}} = T_{i\,\max,\text{old}} + (1/mC)\left[Ak\left(\frac{T_{i\,\max} - T_{i\,\max-1}}{h_{i\,\max}}\right) + h_{\text{tr}}A(T_{i\,\max} - T_\infty) + mL\right] \tag{11}$$

In this way the procedure maps the thinning of the entire film in a given time interval Δt by summing the individual sublayers h_i, each of which has thinned an amount Δh_i according to Equations 5 and 6, while simultaneously tracking the temperature T_i of each sublayer individually according to Equations 8 through 11.

In order to calculate the *Mn* values corresponding to a particular time-step during fluid thinning using Equation 2, the thermal gradient within the surface layer of the fluid must be evaluated. This is performed by a simple fitting procedure of the temperature vs. film-depth profile as depicted in Fig. 4. The temperature profile that develops is nonlinear resulting in a locally-varying temperature gradient (see Fig. 4a). However,

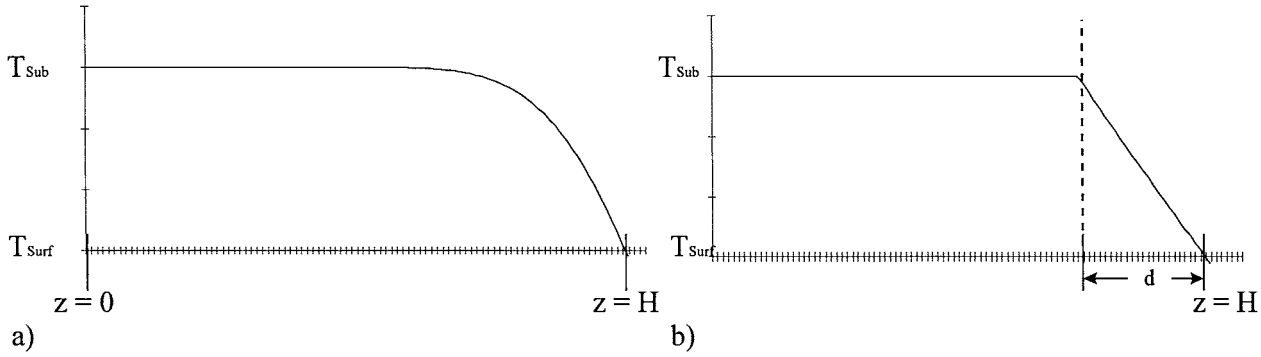

Figure 4 (a) is a typical temperature v. depth profile and (b) is an approximation to (a). The value for d in (b) is the distance from the fluid/air interface into the liquid for which the areas under the two curves are equivalent.

we are interested in the overall effect that this profile has so a reasonable aggregate value is used for the present work. Fig. 4b shows our method. We fix the top surface and substrate temperatures according to those found in the real temperature profile and find an effective depth, d, in a manner equivalent to the analyses of Currie [10] and Vidal and Acrivos [11]. The value for d is the depth into the fluid for which the areas under the curves in Fig. 4a and Fig. 4b are equal. This is the value for d, the thermal penetration depth, placed in Equation 2.

4. Results

Numerical analyses were run for three related fluids of decreasing volatility: methanol, ethanol and 1-propanol. The pertinent physical properties for each of these alcohol solutions are found in Table I. Experimentally determined evaporation rates were used that conformed to earlier studies [17, 18]. Each simulation predicted the behavior of these pure alcohol fluids spun on to a 4 in. diameter substrate rotated at spin speed selected from: 2000, 3000, 4000, and 8000 RPM. The alcohol layers are modeled as being accelerated instantaneously to a given rotation rate from a stagnant, uniform distribution across the entire substrate. Three different initial fluid thickness starting-points were also tested: 1 mm, 0.5 mm, and 0.2 mm. *Mn* values were calculated for each Δt time interval and the results were compared to the critical values as described above.

The effect of initial quantity of fluid dispensed onto the wafer is illustrated by the *Mn* data presented in Fig. 5, showing Ethanol, spinning at 3000 RPM, for three different initial fluid depths. The X-axis is fluid depth as a function of time, so the progression of any of the thinning runs starts at the right and works toward lower H values with increasing time. Thus, the three starting fluid depths each start at points progressively further to the left. All three curves rise up rather rapidly to their peak values and then gradually reduce with time along a nearly identical trajectory. All three dispense amounts result in some time duration where super-critical *Mn* values are experienced by the coating. Since the thicker starting layers rise to higher *Mn* values and spend more time in the super-critical condition, it can be expected that thinner initial fluid thickness will be preferable when making coatings with volatile solvents.

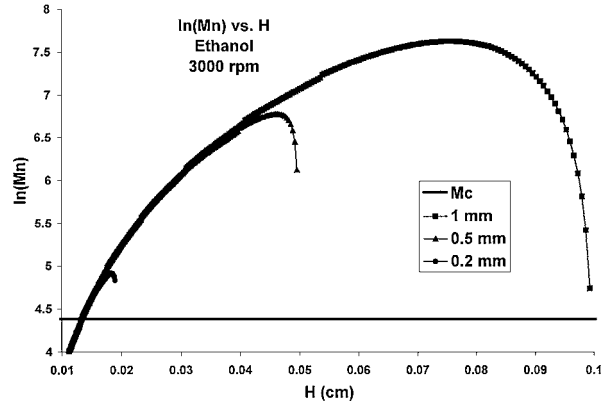

Figure 5 Marangoni number, *Mn*, plotted versus film thickness, H. This figure illustrates the effect of initial quantity of fluid dispensed onto the substrate. Ethanol is being spun at 3000 RPM, starting from initial thicknesses of 0.2, 0.5, and 1.0 mm. Slight discontinuities along each plot indicate points where the mesh size was adjusted by the computer and do not represent real effects. The single nearly-horizontal line shows the critical Marangoni number that applies, according to Nield [13]. Thickness values between about 120 μm and 1 mm are all above the critical threshold and therefore susceptible to thermocapillary convection during those parts of spinning.

TABLE I Physical constants of methanol, ethanol, and propanol

	Methanol	Ethanol	1-Propanol
C_p J/(g · C°)	2.53	2.44	2.39
L kJ/mol	37.43	42.32	47.45
$\frac{\partial\sigma}{\partial T}$ mN/(m · C°)	0.0773	0.0833	0.0776
β 1/C°	1.49×10^{-3}	1.4×10^{-3}	1.22×10^{-3}
k W/(m · C°)	0.2014	0.1704	0.1548
η (N/m^2) · s	0.5938×10^{-3}	1.2164×10^{-3}	2.319×10^{-3}
MW g/mol	32.04	46.07	60.1
ρ g/cm^3	0.7914	.7893	0.8035
C_e (μ/s)(rpm)$^{-1/2}$	0.0688	0.0434	0.0113

All data were found in the *CRC Handbook of Chemistry and Physics*, Vol. 79 [19] except evaporation rate constants (C_e). C_e values for methanol and ethanol come from Ref. 17. C_e for 1-propanol was determined in a manner equivalent to that of Ref. 17.

The effect of solvent volatility is illustrated in Fig. 6, showing data for the three solvents, each spun at 2000 RPM, and starting from 0.5 mm initial depths. It comes as no surprise that more volatile solvents exert substantially greater thermocapillary driving forces during spinning under otherwise identical conditions. With greater volatility comes a greater rate of heat extraction via the latent heat of vaporization and therefore steeper temperature gradients near the surface. This creates greater thermocapillary driving forces.

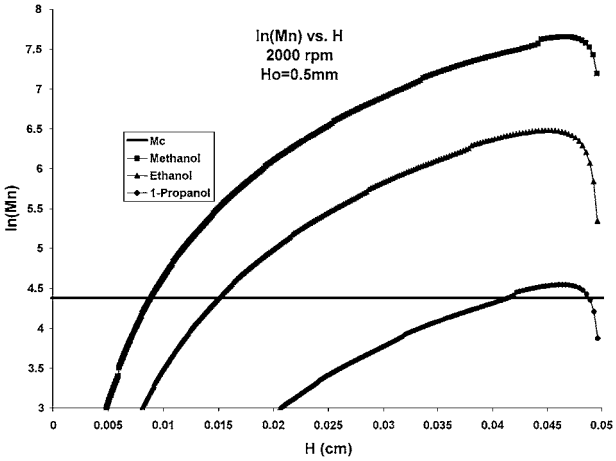

Figure 6 Marangoni number, *Mn*, plotted versus film thickness, *H*. This figure illustrates the effect of solvent volatility on thermocapillary instability level. Methanol, ethanol, and propanol are each spun at 2000 RPM, starting from an initial thickness of 0.5 mm. More volatile solvents exhibit more susceptibility to thermocapillary convection during spin-coating. The propanol barely reaches the critical value indicating that less volatile solvents (with otherwise similar properties) will definitely not experience thermocapillary disturbance.

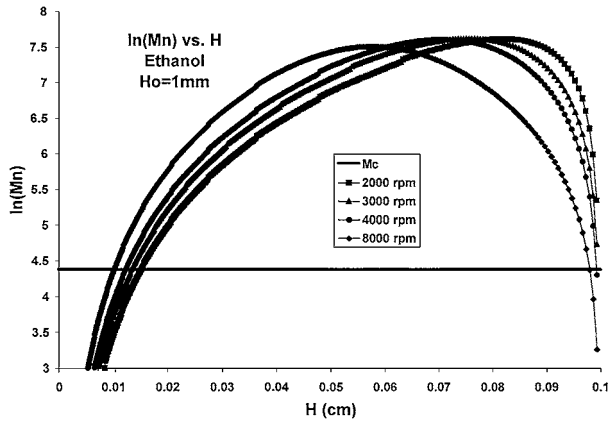

Figure 7 Marangoni number, *Mn*, plotted versus film thickness, *H*. This figure illustrates the effect of spin speed on thermocapillary instability level. Ethanol is used with an initial dispense thickness of 1.0 mm. Spin speeds ranging from 2000 to 8000 RPM have been tested.

Finally, the effect of spin-speed is compared in Fig. 7. Each sample is ethanol starting at 1.0 mm in depth and spinning down at RPM values of 2000, 3000, 4000, and 8000 RPM. It is interesting that the peak *Mn* values are relatively similar even when widely disparate rotation rates are used. The major difference is that when faster spin speeds are used the rise in *Mn* is somewhat slower at the beginning. This is a result of the faster thinning that results at higher spin speed—allowing less *time* for heat removal and therefore thermal gradients that are not as steep comparing equivalent thickness states.

5. Discussion

The numerical model has shown that solutions with more volatile solvents are increasingly susceptible to thermocapillary convection effects during spin coating. Therefore, when designing coating solutions it may be advisable to choose solvents with relatively lower vapor pressures to reduce evaporative cooling driving forces.

It is interesting that the severity of instability is greater for thicker starting layers and at earlier times, when the solution is still at nearly at its starting depth. Thus, by dispensing a smaller amount of fluid it may, in some instances, be possible to avoid thermocapillary instability that might otherwise erupt. The fact that the magnitude of the supercritical condition is smaller with smaller initial film thicknesses is a result of the direct dependence of *Mn* upon H^2 (see Equation 2). Thinner fluid by nature results in smaller *Mn* numbers.

It is somewhat surprising that different spin speeds have little effect on the extent of thermocapillary forces exerted on the fluids. Because of the laminar air flow conditions, the evaporation rate increases as the square root of spin speed [17, 18]. So, the faster evaporation rate at higher spin speed is almost completely counterbalanced by the reduced time for the thermal gradient to develop during spinning.

6. Conclusions

In this study we have utilized a simple numerical analysis in order to simulate the thinning behavior and temperature profile of several spun-on alcohol solutions. The solutions are in thermal equilibrium with their surroundings at the onset of spinning and are subsequently subjected to thermal gradients that arise as a result of evaporative cooling. By consistently mapping the depth and thermal behavior of these spinning solutions we are able to generate instantaneous values of the Marangoni number, *Mn*, which describes the stability condition of a correspondingly thin layer of stagnant fluid subjected to otherwise equivalent physical conditions. Comparison of these results with those of past studies determines the likelihood that convection cells would develop within these similar stagnant fluids and thereby indicate the potential development of striations across the rotating fluid.

Our results indicate that evaporative cooling is significant enough to trigger the onset of thermocapillary driven convection within sufficiently thick fluid layers or within layers that have large enough volatility. Simulations run for all three alcohol solutions indicate that for an initial fluid layer deposited 1 mm thick, thermocapillary instabilities are sufficient for the onset of convection regardless of spin speed. Fluid layers deposited at an initial thickness of 0.5 and 0.2 mm thick the significance of any thermocapillary instability increases with increasing spin speed/evaporation rate. Thus thermocapillary instabilities can be considered a potential source for the onset of striations within spun-on alcohol solutions. Future work will examine composition dependent effects driven by solvent evaporation.

Acknowledgements

The authors would like to thank the National Science Foundation for providing the funding necessary for this research under grant DMR 98-02334. We are also appreciative of Specialty Coating Systems for the use of their spin coater during these analyses.

References

1. D. P. BIRNIE, III, B. J. J. ZELINSKI, S. P. MARVEL, S. M. MELPOLDER and R. RONCONE, *Optical Engineering* **31** (1992) 2012.

2. D. P. BIRNIE, III, B. J. J. ZELINSKI and D. L. PERRY, *ibid*. **34** (1995) 1782.
3. P. FRASCH and K. H. SAREMSKI, *IBM J. Res. Develop*. **26**(5) (1982) 561.
4. X. M. DU, X. ORIGNAC and R. M. ALMEIDA, *J. Amer. Ceram. Soc*. **78**(8) (1995) 2254.
5. M. J. BLOCK, *Nature* **178** (1956) 650.
6. J. R. A. PEARSON, *J. Fluid Mech*. **4** (1958) 489.
7. H. BÉNARD, *Rev. Gen. Sci. Pures Appl. Bull Assoc. Franc. Avan. Sci*. **11** (1900) 1261.
8. E. L. KOSCHMEIDER, *Adv. Chem. Phys*. **26** (1974) 177.
9. L. RAYLEIGH, *Phil. Mag*. **32**(6) (1916) 529.
10. I. G. CURRIE, *J. Fluid Mech*. **29** (1967) 337.
11. A. VIDAL and A. ACRIVOS, *I & EC Fundamentals* **7**(1) (1968) 53.
12. B. K. DANIELS, C. R. SZMANDA, M. K. TEMPLETON and P. TREFONAS III, *Advances in Resist Technology and Processing III* **631** (1986) 192.
13. D. A. NIELD, *J. Fluid Mech*. **19** (1964) 341.
14. D. E. HAAS, J. N. QUIJADA, S. J. PICONE and D. P. BIRNIE, III, in "Sol-Gel Optics V," edited by B. S. Dunn, E. J. A. Pope, H. K. Schmidt and M. Yamane, *Proc. SPIE* **3943** (2000) 280.
15. A. G. EMSLIE, F. T. BONNER and L. G. PECK, *J. App. Physics* **29**(5) (1958) 858.
16. E. C. COBB and O. A. SAUNDERS, *Proc. R. Soc*. **236** (1956) 343.
17. D. P. BIRNIE, III and M. MANLEY, *Phys. Fluids* **9**(4) (1997) 870.
18. F. KREITH, J. H. TAYLOR and J. P. CHONG, *J. Heat Transfer* May (1959), 95.
19. "CRC Handbook of Chemistry and Physics," 79th ed. (CRC Press 1998).

Received 9 October 2000
and accepted 21 December 2001